Preprints of the 21st IFAC World Congress (Virtual)
Berlin, Germany, July 12-17, 2020

# A steady-state model of the high-pressure grinding rolls

**Alex Thivierge** *,*** **Jocelyn Bouchard** * **André Desbiens** **

*LOOP, Centre E4m, Université Laval, Quebec City, Canada*
* *Department of Chemical Engineering*
** *Department of Electrical and Computer Engineering*
*** *Corresponding author: alex.thivierge.1@ulaval.ca*

**Abstract:**
This paper presents a steady-state model of the high-pressure grinding rolls (HPGR) based on population balance methods. It simulates the power draw, flow rate, and particle size distribution of both the edge and center products from the operating pressure, rotating speed, and size-by-size feed rates. Upgrades from previous work include the addition of the edge cutter setting (in distance unit) as an input parameter, and the equation for the variation of density along the rolls width to account for inaccuracy in throughput prediction generally compensated using an extrusion or slip correction factor. Results appear qualitatively coherent, but remain to be validated with experimental data.

*Keywords:* High-pressure grinding rolls, phenomenological modeling, mineral processing

## 1. INTRODUCTION

The minerals industry accounts for approximately 11% of the total energy consumption (McLellan et al., 2012), and 53 % of this share comes from comminution processes (CEEC, 2013). Napier-Munn (2015) listed different ways to reduce this amount including novel flowsheets and improved process control. Simulation environments allow studying these solutions without the risks associated with expensive plant trials, but require process unit models.

This paper presents a steady-state high-pressure grinding rolls (HPGR) model, which could be used in such applications, even if process dynamics are neglected. This unit operation indeed exhibits a very short residence time compared to that of the secondary grinding circuit, thus allowing considering it as a static process, providing the simulation step is sufficiently long.

The manuscript first introduces the model workflow. A simulation example is then presented. Follows a discussion about the model advantages and limitations.

## 2. HPGR MODEL

Fig. 1 shows the general structure of the model. Empirical models allow estimating key variables (operating gap and extrusion density), and the rest of the simulation workflow makes use of a modular approach following the work of Torres and Casali (2009) and Morrell et al. (1997a).

### 2.1 Grinding pressure

The HPGR has two operating settings: the hydraulic operating pressure $P_o$, and the rolls tangential speed $\eta$. $P_o$ is linked to the grinding force $F$ applied to the floating roll through the hydraulic system with:

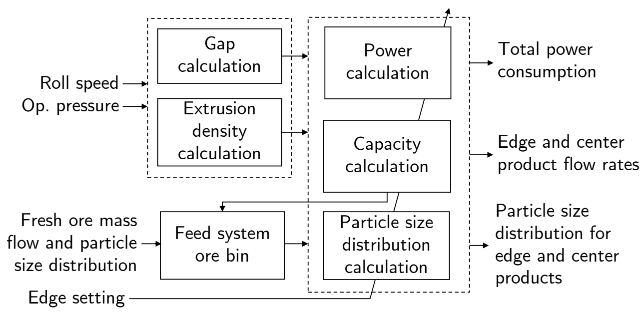


Fig. 1. Simplified schematic of the HPGR model structure

$$F = P_o\, A, \tag{1}$$

where $A$ is the total area of the hydraulic pistons. The ratio:

$$\tilde{F} = \frac{F}{D\,L} \tag{2}$$

defines the specific force $\tilde{F}$, where $D$ and $L$ are the diameter and width of the rolls, respectively.

Although the set-point of $P_o$ is manipulated, it is actually the grinding pressure that acts on the material bed. It cannot be measured directly, but Klymowsky et al. (2002) proposed estimating its average (along both $y$ and $z$ axis) using:

$$\bar{P}_{m_{y,z}} = \frac{F}{\frac{D}{2}\bar{\alpha}_c\, L}, \tag{3}$$

where $\bar{\alpha}_c$ is the average nip angle along the roll (i.e. the arithmetic mean of Eq. (12), see below). The grinding pressure is known to vary along the roll and gap as shown

 

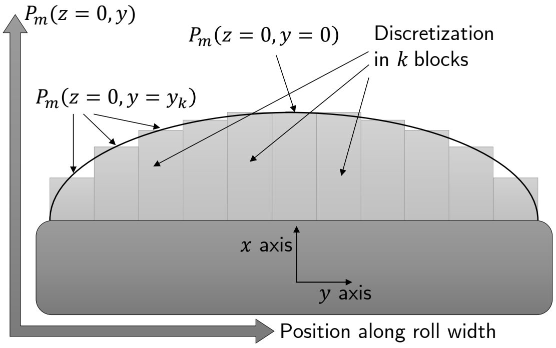


Fig. 2. Grinding pressure $P_m$ distribution along the roll

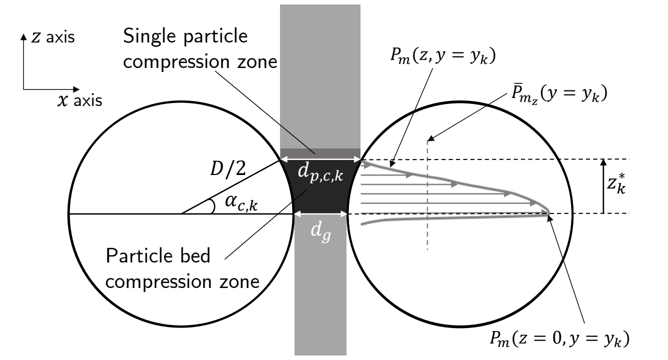


Fig. 3. Grinding pressure $P_m$ distribution along the gap, showing also $d_g$, the operating gap, $D/2$, the radius of the rolls, along with $\alpha_{c,k}$, the nip angle, $d_{p,c,k}$ the critical size, and $z_k^*$, the height at the beginning of the bed particle compression zone in block $k$

in Fig. 2 and 3 (Klymowsky et al., 2002). The model accounts for the distribution by considering $k$ discrete blocks along the width as shown in Fig. 2.

Along the $z$ axis, the maximum pressure occurs right before the extrusion at $z = 0$, i.e. inside the operating gap. The average (along the $y$ axis) is:

$$\bar{P}_{m_y}(z=0) = \frac{F}{c\,\bar{\alpha}_c DL} \approx 2.5\bar{P}_{m_{y,z}}, \tag{4}$$

with $0.18 < c < 0.23$ (Klymowsky et al., 2002). In this work, it is assumed that this relation also holds true in each discretized block $k$ along the $y$ axis:

$$P_m(z=0, y=y_k) = \frac{F_k}{c\,\alpha_{c,k} DL_k} \approx 2.5\bar{P}_{m_z}(y=y_k), \tag{5}$$

where $\bar{P}_{m_z}(y=y_k)$ is the grinding pressure average along the $z$ axis in each block, $y_k$ is the relative position on the $y$ axis of the block $k$ and ranges from $\frac{-L}{2}$ to $\frac{L}{2}$, $F_k$ is the grinding force applied on block $k$ with length $L_k$, and $\alpha_{c,k}$ is the nip angle in block $k$. Lubjuhn (1992) proposed an equation to model the pressure in the gap along the roll ($y$ axis) for a laboratory scale HPGR:

$$\frac{P_m(z=0,y=y_k)}{P_m(z=0,y=0)} = 1 - \left(2\left|\frac{y_k}{L}\right|\right)^{1.6}. \tag{6}$$

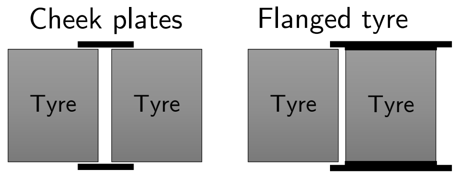


Fig. 4. Top view showing cheek plates and flanges configurations (Adapted from Knorr et al., (2013))

For larger HPGR's, the pressure distribution is expected to be different because of the reduction of the edge effect (Van der Meer, 2010). From discrete element method simulation results, Johansson and Evertsson (2019) concluded that the pressure distribution should instead plateau for most of the roll as:

$$\frac{P_m(z=0,y=y_k)}{P_m(z=0,y=0)} = \min\left(4 - 4\left(2\frac{y_k}{L}\right)^2; 1\right). \tag{7}$$

It is noted that Eq. (6) and (7) apply only if cheek plates are used on the HPGR as a different pressure profile is expected with flanges (Knorr et al., 2013). These alternative mechanisms, cheek plates being attached to the frame, and flanges, to the rolls are depicted in Fig. 4.

### *2.2 Working gap*

The working gap width $d_g$ varies according to the force applied. Morrell et al. (1997a) showed that:

$$\frac{d_g}{D} = k_5\left(k_1\eta^2\psi + k_2\eta\sqrt{\psi} + k_3\right)\left(1 + k_4\log\tilde{F}\right), \tag{8}$$

where $\psi = \frac{2}{g\,D}$, $g$ is the gravitational acceleration constant, and $k_1$ to $k_5$ are empirical parameters. $k_5$ is used to account for different moisture content, feed top size, type of rolls, and machine size (scale-up factor).

### *2.3 Extrusion density*

Austin et al. (1993) proposed the following empirical relationship to model the average porosity of the material in the gap $\theta_g$ :

$$(1-\theta_g) - (1-\theta_0) = k_6(\tilde{F})^{k_7}, \tag{9}$$

where $\theta_0$ is the average porosity in the feed material, with empirical parameters $k_6$ and $k_7$. Multiplying this equation by the solid density, and rearranging the terms lead to:

$$\rho_g = k_8(\tilde{F})^{k_7} + \rho_b, \tag{10}$$

where $\rho_g$ is the average density of the material in the gap and $\rho_b$ is the bulk density of the ore. Assuming compaction is actually function of the pressure exerted on the particle bed, i.e. $P_m(z=0, y=y_k)$, the density distribution in the gap varies with blocks along roll width as:

$$\rho_{g,k} = k_9(P_m(z=0,y=y_k))^{k_{10}} + \rho_b. \tag{11}$$

### 2.4 Nip angle

The steady-state momentum balance is used to calculate the nip angle (shown in Fig. 3) as a function of the ore density in the extrusion zone (Morrell et al., 1997a). For each $k$ block, it is:

$$\alpha_{c,k} = \arccos\left(\frac{1}{2D}\left(\phi + \sqrt{(\phi)^2 - \frac{4d_g\rho_{g,k}D}{\rho_b}}\right)\right), \quad (12)$$

with $\phi = d_g + D$.

It is noted that all unknowns $F_k$, $P_m(z = 0, y = y_k)$, $P_g(z = 0, y = 0)$, $d_g$, $\rho_{g,k}$, and $\alpha_{c,k}$ are found simultaneously by solving the system of equations comprised of Eq. (5), (6) or (7) depending on HPGR size, (8), (11), (12), and:

$$F = \sum_{k=1}^{n_k} F_k, \quad (13)$$

where $n_k$ is the total number of blocks.

### 2.5 Capacity

Applying a mass balance at the extrusion zone provides the equation of continuity (Daniel and Morrell, 2004):

$$\dot{M} = \rho_g\, d_g\, \eta\, L, \quad (14)$$

where $\dot{M}$ is the mass flow rate. This equation is also true on each block, therefore the throughput can be defined as:

$$\dot{M} = \sum_{k=1}^{n_k} \dot{M}_k = \sum_{k=1}^{n_k} \rho_{g,k}\, d_g\, \eta\, \frac{L}{n_k}, \quad (15)$$

where $\dot{M}_k$ is the production rate in each block section.

### 2.6 Power draw

The total power draw of a single roll $\dot{W}_{sr}$ is defined by (Klymowsky et al., 2002):

$$\dot{W}_{sr} = \omega\, T, \quad (16)$$

where $\omega$ is the rotation speed (rad/s) (i.e. $\omega = \frac{2\eta}{D}$), and $T$ is the total torque applied on the roll:

$$T = T_G + T_0, \quad (17)$$

where $T_0$ is the no-load torque, i.e. required to rotate the rolls without processing mineral, and $T_G$ is the torque caused by the grinding force. $T_0$ should be constant because the HPGR behaves as a constant load machine (Numbi and Xia, 2015), and $T_G$ is found with a free body diagram as:

$$T_G = \sum_{k=1}^{n_k} F_k \sin(\beta_k)\, \frac{D}{2}, \quad (18)$$

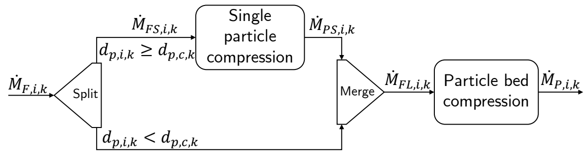


Fig. 5. Calculation work flow for the two stages of compression

where $\beta_k$ is the angle at which the grinding force is applied. According to Klymowsky et al. (2006): $\beta \approx \frac{\bar{\alpha}_c}{2}$, thus the torque resulting from the grinding action is:

$$T_G \approx \sum_{k=1}^{n_k} F_k \sin\left(\frac{\alpha_{c,k}}{2}\right) \frac{D}{2}, \quad (19)$$

which must be multiplied by 2 to obtain the combined torque of both rolls. Therefore, the grinding power, or the net power consumption per block is:

$$\dot{W}_{N,k} = 2F_k \sin\left(\frac{\alpha_{c,k}}{2}\right)\eta, \quad (20)$$

and the total power draw of the HPGR is:

$$\dot{W} = 2\,\omega\, T = \frac{4\eta}{D}(T_G + T_0). \quad (21)$$

### 2.7 Particle size distribution

A population balance describes the particle size distribution of the HPGR product. Two grinding mechanisms are assumed to exists: single particle compression, and bed particle compression grinding as shown on Fig 3.

The proposed model is largely inspired by the work of Torres and Casali (2009) but introduces the following updates: (1) a subdivision of the single compression zone to account for every block, (2) a varying hold up along blocks, and (3) upgraded breakage and selection functions. Fig. 5 illustrates the calculation work flow. If the particle size in class $i$ and block $k$ $d_{p,i,k}$ is greater than the critical size $d_{p,c,k}$ shown in Fig 3, then it will break through single particle compression before undergoing particle bed compression. The material feeding the second grinding zone $\dot{M}_{FL,i,k}$ is therefore the sum of the mass flow rate of initial material smaller than $d_{p,c,k}$ and the product of the single particle compression grinding in class $i$ and block $k$ ($\dot{M}_{PS,i,k}$). The critical size in each block is derived from a steady-state momentum balance as:

$$d_{p,c,k} = d_g + D\left(1 - \cos(\alpha_{c,k})\right). \quad (22)$$

The particles in block $k$ and size class $i$ greater than $d_{p,c,k}$ will break according to the breakage matrix:

$$\dot{M}_{PS,i,k} = \sum_{l=1}^{n_i} b_{i,l}\dot{M}_{FS,l,k}, \quad (23)$$

where $b_{i,l}$ is the breakage matrix coefficients, $\dot{M}_{FS,l,k}$ is the particle size distribution of the HPGR feed in block $k$, and $n_i$ is the number of size classes.

The particle bed compression grinding zone assumes plug flow of particles, hence the mass balance along the height of the zone is (Torres and Casali, 2009):

$$v_z \frac{d}{dz} m_{i,k}(z) = \sum_{j=1}^{i-1} s_{j,k} b_{i,j} m_{j,k}(z) - s_{i,k} m_{i,k}(z), \qquad (24)$$

where $v_z$ is the vertical speed of particles at height level $z$, $m_{i,k}$, the mass of particles of size class $i$ in block $k$, $s_{i,k}$, the $i,i$ element of the diagonal selection matrix for the $k$ block, i.e. the rate at which a particle of size $i$ is fragmented, and $b_{i,j}$, the $i,j$ coefficient of the breakage matrix. As proposed by Torres and Casali (2009), both grinding zones use the same breakage matrix.

The previous differential equation has an analytic solution (Reid, 1965) from border conditions:

$$\frac{d}{dt} m_{i,k}(z = z_k^*) = \dot{M}_{FL,i,k},$$

and

$$\frac{d}{dt} m_{i,k}(z = 0) = \dot{M}_{P,i,k},$$

where $z_k^*$ is the height at the beginning of the bed particle compression zone, and $\dot{M}_{P,i,k}$, the HPGR product mass flow rate of size $i$ in block $k$. The value of $z_k^*$ is found geometrically as shown in Fig. 3 (Torres and Casali, 2009):

$$z_k^* = \frac{D}{2} \sin(\alpha_{c,k}). \qquad (25)$$

The analytic solution of Eq. (24) is (Torres and Casali, 2009):

$$\dot{M}_{P,i,k} = \sum_{j=1}^{i} a_{i,j,k} \exp\left(-s_{j,k}\, \tau_k\right), \qquad (26)$$

where $\tau_k$ is the residence time in block $k$, and $a_{i,j,k}$ is:

$$a_{i,j,k} = \begin{cases} 0 & \text{if } i < j \\ \displaystyle\sum_{l=j}^{i-1} \frac{b_{i,l} s_{l,k}}{s_{i,k} - s_{j,k}} & \text{if } i > j \\ \displaystyle\dot{M}_{FL,i,k} - \sum_{l=1}^{i-1} a_{i,j,k} & \text{if } i = j. \end{cases}$$

The breakage and selection matrix are calculated through their respective function. Torres and Casali (2009) used a normalized breakage function. More recently, Anticoi et al. (2018) performed piston press particle bed compression tests and noticed that the breakage function was not always normal depending on the ore. Hence, the model here makes use of the non-normalized breakage function from Austin and Luckie (1972), with the matrix cumulative coefficients:

$$b_{i,j}^* = K_i \left(\frac{d_{p,i}}{d_{p,j}}\right)^{h_2} + (1 - K_i)\left(\frac{d_{p,i}}{d_{p,j}}\right)^{h_3} \qquad (27)$$

with

$$K_i = h_1 \left(\frac{d_{p,i}}{h_5}\right)^{h_4}, \qquad (28)$$

where $h_1$ to $h_5$ are empirical parameters. If the breakage function is normal, then $h_4$ becomes 0. $b_{i,j}^*$ is the breakage matrix coefficients expressed in cumulative form. The discrete breakage matrix coefficient $b_{i,j}$ are:

$$b_{i,j} = b_{i-1,j}^* - b_{i,j}^*. \qquad (29)$$

Herbst and Fuerstenau (1980) defined the elements of the energy-based selection function $s_i^E$ as:

$$\ln\left(\frac{s_i^E}{S_1^E}\right) = \zeta_1 \ln\left(\frac{\overline{d}_{p,i}}{\overline{d}_{p,1}}\right) + \zeta_2 \left(\ln\left(\frac{\overline{d}_{p,i}}{\overline{d}_{p,1}}\right)\right)^2, \qquad (30)$$

where $\zeta_1$, $\zeta_2$ et $S_1^E$ are empirical parameters. $\overline{d}_{p,1}$ and $\overline{d}_{p,i}$ are the average size in class 1 (coarsest) and $i$, respectively. For each block $k$, the elements of the diagonal selection matrix are estimated considering an energy dissipation factor $\gamma$ (Fuerstenau et al., 1991):

$$s_{i,k} = \frac{\dot{W}_{N,k}}{\left(\dot{W}_{N,k}/\dot{M}_k\right)^{\gamma}} s_i^E. \qquad (31)$$

At steady-state, the hold up will depend on the residence time of each block which is found using geometry, as:

$$\tau_k = \arcsin\left(\frac{2z_k^*}{\sqrt{D}}\right)\frac{\sqrt{D}}{2\eta} \approx \frac{z_k^*}{\eta}. \qquad (32)$$

Summing along the $n$ blocks provide the total mass flow rate in class $i$:

$$\dot{M}_{P,i} = \sum_{k=1}^{n_k} \dot{M}_{P,i,k}. \qquad (33)$$

The edge flow rate per class:

$$\dot{M}_{E,i} = \sum_{k\,\in\,\Gamma} \dot{M}_{P,i,k} \qquad (34)$$

allows estimating the total edge flow rate as:

$$\dot{M}_E = \sum_{k\,\in\,\Gamma} \dot{M}_k, \qquad (35)$$

where the $\Gamma$ set contains the blocks in edge area, i.e. the blocks delimited by the edge cutter positions.

### *2.8 HPGR feed bin*

A variable transport delay models the feed system bin as a function of ore level.

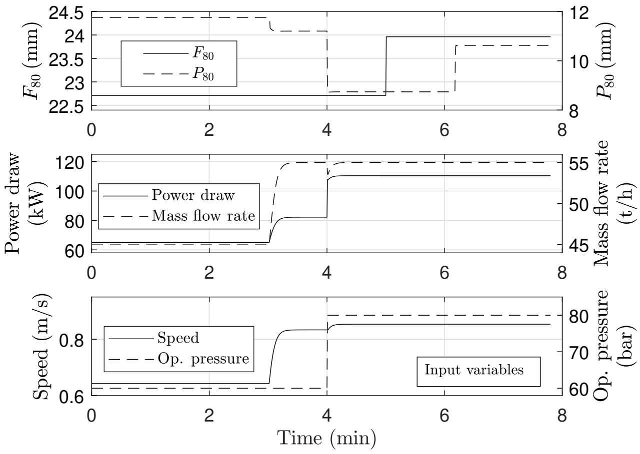


Fig. 6. Simulation results

## 3. SIMULATION

Fig. 6 presents a simulation example in which a PI controller keeps the feed bin level constant by varying the rolls speed. Three cases are simulated: fresh ore feed rate to the HPGR bin inlet variation (+10 t/h step change at $t = 3$ min), operating pressure set-point step change ($t = 4$ min), and inlet ore size disturbance (increased sieve dimension greater than 80% of feed particles ($F_{80}$) at $t = 5$ min).

Speed and pressure both increase power draw significantly. The former has a large effect on the processing rate, but very little on the sieve dimension greater than 80% of product particles ($P_{80}$), while the latter has the opposite effects. The effect of increasing the pressure on the mass flow rate is explained by the decreasing working gap. Increasing the speed slightly reduces the $P_{80}$ as explained by the relationship between the selection function and the power draw (Eq. (31)). These results are consistent with the experimental observations of Lim et al. (1997).

As expected, feeding a coarser, but equally hard, ore results only in an increased $P_{80}$. It affects neither the mass flow rate, nor the power draw.

## 4. DISCUSSION

More data are needed to validate the grinding pressure distributions used in this model (Eq. (6) and (7)). Indeed, Lubjuhn (1992) developped his model from a lab scale HPGR, equipped with only three sensors, and assuming symmetry. Also, the pressure distribution for industrial scale HPGR's was derived from discrete element modeling rather than from actual measurements (Johansson and Evertsson, 2019). Back-calculating the grinding pressure distribution from test data, using different edge settings and this simulation framework, should cast some light on this issue.

Regarding the gap prediction, only the speed and pressure are considered in Eq. (8), which limits the range of application in simulation studies. As an example, Fig. 7 depicts the important effect of moisture on the measured working gap during HPGR pilot scale tests carried out by Weir Minerals. The feed particle size is also expected to display a significant effect, as it is known to influence particle bed compaction behavior (Hosten and Cimilli, 2009). This requires further work.

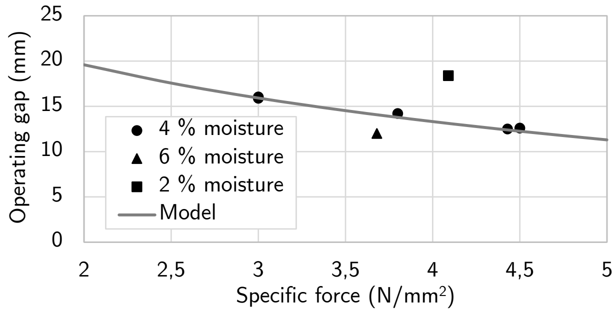


Fig. 7. Eq. (8) predictions with 4 % moisture content and $k_5 = 1$

Campos et al. (2019) and Morrell et al. (1997b) found the basic continuity equation to sometimes be inaccurate for mass flow prediction, and proposed slip or extrusion factors to account for discrepancies. However, Schönert and Sander (2002) showed that no slip was possible inside the gap. The model presented in this paper is in agreement with these findings. It is expected that the lack of precision of the continuity equation will be corrected by considering the extrusion density distribution along the roll width as in Eq. (15).

The proposed power model is different from the one published by Torres and Casali (2009):

$$\sum_{k=1}^{n_k} \dot{W}_{N,k} = P_o D L \eta \sin\left(\frac{\bar{\alpha}_c}{2}\right), \tag{36}$$

which has been used extensively (e.g. by Hasanzadeh and Farzanegan (2011) and Numbi and Xia (2015)). Although this equation seemed to be adequate in its original paper, Campos et al. (2019) introduced a correction factor to explain more recent experimental results. This model attempt to explain the discrepancy in a different manner, albeit validation work still needs to be undertaken: (1) a piston area converts operating pressure to grinding force explicitly, (2) the area where the grinding pressure is applied is only the nipping area as opposed to the whole top half, and (3) the material density in the extrusion zone changes according to the position along the roll.

Figure 8 depicts data from Austin et al. (1993). The remaining material in the coarsest sieve class after HPGR grinding is plotted as a function of the specific energy consumption, which was manipulated by varying the hydraulic pressure. Both the breakage rate models used in Torres and Casali (2009) (without $\gamma$) and the one used here are calibrated on the data set. The quality of the fit indicates that using the energy dissipation factor increases the accuracy of the breakage rate model as suggested by Fuerstenau et al. (1991).

## 5. CONCLUSION

This paper presented a general framework of a steady-state HPGR model that considers the edge setting as an input parameter. The calculation workflow involves esti-

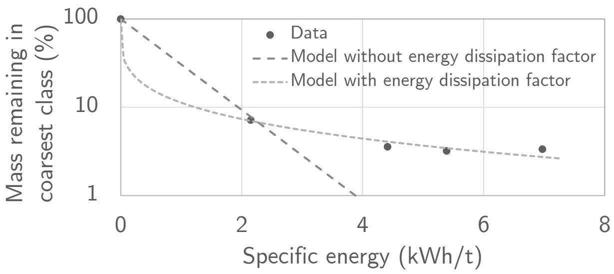


Fig. 8. Effect of the energy dissipation factor $\gamma$

mating a density distribution to account for the previous inaccuracies in mass flow and power draw predictions.

Future work will include quantifying the effect of the moisture and feed particle size on the working gap and extrusion density distribution, validating the capacity and power models, and calibrating the model. The simulator will then be used along with grinding and flotation models (Thivierge et al., 2019) to study the issue of designing and controlling HPGR circuits to increase the economic performance, and reduce energy consumption.

## 6. ACKNOWLEDGMENTS

The authors would like to acknowledge the financial support of Nemaska Lithium, the Fonds verts and Fonds de Recherche du Québec – Nature et Technologies (FRQNT) partnership, Natural Sciences and Engineering Research Council of Canada (NSERC), and the SAG Conference Award Foundation. The authors would also like to thank Serhat Onol and Henning Knapp from Weir Minerals for sharing the HPGR pilot test data set.

## REFERENCES

Anticoi, H., Guasch, E., Hamid, S., Oliva, J., Alfonso, P., Garcia-Valles, M., Bascompta, M., Sanmiquel, L., Escobet, T., Argelaguet, R., et al. (2018). Breakage function for HPGR: mineral and mechanical characterization of tantalum and tungsten ores. *Minerals*, 8(4), 170.

Austin, L. and Luckie, P. (1972). The estimation of non-normalized breakage distribution parameters from batch grinding tests. *Powder Technology*, 5(5), 267 – 271.

Austin, L., Weller, K., and Lim, W. (1993). Phenomenological modelling of the high pressure grinding rolls. In *18th International Mineral Processing Congress, Sydney, Australia*, 87–96.

Campos, T.M., Bueno, G., Barrios, G.K., and Tavares, L.M. (2019). Pressing iron ore concentrate in a pilot-scale HPGR. Part 2: Modeling and simulation. *Minerals Engineering*, 140, 105876.

CEEC (2013). Innovation – mining more for less. Report, Coalition for energy efficient comminution. URL `www.ceecthefuture.org/comminution-2/innovation-mining-less/`.

Daniel, M.J. and Morrell, S. (2004). HPGR model verification and scale-up. *Minerals Engineering*, 17(11-12), 1149–1161.

Fuerstenau, D., Shukla, A., and Kapur, P. (1991). Energy consumption and product size distributions in choke-fed, high-compression roll mills. *International Journal of Mineral Processing*, 32(1-2), 59–79.

Hasanzadeh, V. and Farzanegan, A. (2011). Robust HPGR model calibration using genetic algorithms. *Minerals Engineering*, 24(5), 424–432.

Herbst, J. and Fuerstenau, D. (1980). Scale-up procedure for continuous grinding mill design using population balance models. *International Journal of Mineral Processing*, 7(1), 1–31.

Hosten, C. and Cimilli, H. (2009). The effects of feed size distribution on confined-bed comminution of quartz and calcite in piston-die press. *International Journal of Mineral Processing*, 91(3-4), 81–87.

Johansson, M. and Evertsson, M. (2019). A time dynamic model of a high pressure grinding rolls crusher. *Minerals Engineering*, 132, 27–38.

Klymowsky, R., Patzelt, N., Knecht, J., and Burchardt, E. (2002). Selection and sizing of high pressure grinding rolls. *Mineral processing plant design, practice and control proceedings*, 1, 636–668.

Klymowsky, R., Patzelt, N., Knecht, J., and Burchardt, E. (2006). An overview of HPGR technology. *the Proceedings of SAG*, 11–26.

Knorr, B., Herman, V., and Whalen, D. (2013). HRC$^{\mathrm{TM}}$: taking HPGR efficiency to the next level by reducing edge effect. *Procemin 2013*.

Lim, W., Campbell, J., and Tondo, L. (1997). The effect of rolls speed and rolls surface pattern on high pressure grinding rolls performance. *Minerals engineering*, 10(4), 401–419.

Lubjuhn, U. (1992). *Materialtransport und Druckverteilung im Spalt der Gutbett-Walzenmühle*. Ph.D. thesis, VDI-Verlag.

McLellan, B., Corder, G., Giurco, D., and Ishihara, K. (2012). Renewable energy in the minerals industry: a review of global potential. *Journal of Cleaner Production*, 32, 32–44.

Morrell, S., Lim, W., Shi, F., and Tondo, L. (1997a). Modelling of the HPGR crusher. *Comminution Practices*, 117–126.

Morrell, S., Shi, F., and Tondo, L. (1997b). Modelling and scale-up of high pressure grinding rolls. In *Proc. XX International Mineral Processing Congress*.

Napier-Munn, T. (2015). Is progress in energy-efficient comminution doomed? *Minerals Engineering*, 73, 1–6.

Numbi, B.P. and Xia, X. (2015). Systems optimization model for energy management of a parallel HPGR crushing process. *Applied Energy*, 149, 133–147.

Reid, K.J. (1965). A solution to the batch grinding equation. *Chemical Engineering Science*, 20(11), 953–963.

Schönert, K. and Sander, U. (2002). Shear stresses and material slip in high pressure roller mills. *Powder technology*, 122(2-3), 136–144.

Thivierge, A., Bouchard, J., and Desbiens, A. (2019). Modeling the net product value of a grinding-flotation circuit. In *Proceedings of the 18th IFAC Symposium on Control, Optimization and Automation in Mining, Mineral and Metal Processing, Stellenbosh, South Africa*.

Torres, M. and Casali, A. (2009). A novel approach for the modelling of high-pressure grinding rolls. *Minerals Engineering*, 22(13), 1137–1146.

Van der Meer, F.P. (2010). High pressure grinding rolls scale-up and experiences. In *XXV International Mineral Processing Congress (IMPC), Brisbane*, 1319–1331.